Available online at www.sciencedirect.com
ScienceDirect
Ceramics International 38 (2012) 967–971
CERAMICS INTERNATIONAL
www.elsevier.com/locate/ceramint

# Refractory filler sands with core–shell composite structure for the taphole nozzle in slide-gate system of steel ladles

Tzu-Tsung Tseng, Hong-Mao Wu, Chun-Nan Chen, Chia-Chin Cheng, Jun-Yen Uan, Weite Wu, Wenjea J. Tseng *

*Department of Materials Science and Engineering, National Chung Hsing University, 250 Kuo Kuang Road, Taichung 402, Taiwan*

Received 26 April 2011; received in revised form 30 July 2011; accepted 1 August 2011
Available online 17 August 2011

**Abstract**

Refractory sand used for filling the taphole nozzle in slide-gate system of steel ladle needs to form a suitable sintered crust to prevent molten metal from direct contact with the gate system which, when opened, permits flow of metal from the ladle through the taphole well. Conventional filler sand consists of powdered mixtures of at least two compositions with suitable particle size and mass ratio. We herein propose a novel core–shell-structured composite particle as the refractory sand. Silicon carbide (SiC) particles with an average diameter of 50 μm were oxidized in air at 1100–1600 °C to form SiC@$SiO_2$ core–shell structure. As the oxidation temperature increases, silica weight-ratio increases from 0.8 to 7.9 wt.%, equivalent to a calculated shell thickness of 20–157 nm, respectively. The crust thickness can be tailored by adjusting the shell thickness. X-ray photoelectron spectroscopy, X-ray diffractometry, and scanning electron microscopy were used to characterize the core–shell structure.


*Keywords:* SiC; Core–shell structure; Refractory; Steelmaking; Composite

## 1. Introduction

Ladle for holding and teeming molten metal often utilizes refractory sands as a particulate barrier and thermal insulator to separate the molten metal from direct contact with gate system in metallurgical operations. The refractory sands are interposed in the drain well of ladle, between the slide-gate nozzle and the molten metal, and are capable of forming a suitable sintered crust in the upper taphole nozzle to prevent permeation of the molten metal during metal-refining process [1,2]. Major properties required for the filler sands include refractoriness, particle-size distribution, suitable particle-packing density, low thermal expansion, low angle of repose, and above all, the ability to form sintered crust with an appropriate thickness when brought in direct contact with the molten metal. When the slide gate is opened upon completion of the refining process, molten metal simply flushes out the filler sands by the pressurized weight, permitting the metal to flow quickly through the well nozzle for subsequent casting process [3].

Use of powdered mixture as the refractory filler sand was first proposed by Kono and Fukuhisa [4] in which, the mixture consisted of predominately high purity silica sands and low-melting additives. Pan and Ko [1] reported that additives such as alkali feldspar would melt and form glassy phase when mixed with silica particles upon contact with molten steel, forming sintered crust at the interface to inhibit permeation of the molten steel during the ladle-refining process. Contact angle and softening temperature of the alkali feldspar were found critically important to the formation of an appropriate sintered crust at elevated temperatures [5]. An improved opening rate without clogging at the slide gate was reported when the silica/feldspar ratio, particle-size distribution, and chemical composition can be fine tuned to a satisfactory level [2]. In addition to the use of silica as the major composition for filler sands, chromite- and zircon-based sands consisting of highly refractory oxide particles mixing with silica and/or other low-melting additives such as the alkali feldspar have also been used extensively. The chromite phase, for example, is difficult to react with molten steel and serves as a particulate backbone when brought in contact with the molten steel. The low-melting phases form glassy phase with the molten steel and fill into the interstices of the packing chromite particles, so that a

* Corresponding author. Tel.: +886 4 2287 0720; fax: +886 4 2285 7017.
*E-mail address:* wenjea@dragon.nchu.edu.tw (W.J. Tseng).

0272-8842/$36.00 
doi:10.1016/j.ceramint.2011.08.017

sufficiently dense layer is formed that prohibits liquid steel from further penetration.

In view of the literature [1,2,4,5], all the refractory sands used for filling the taphole nozzle in a slide-gate system of steel ladle are mixture of powders of different chemical compositions in various weight ratios and particle sizes. At least one composition is required to react with molten steel favorably and form viscous glass at elevated temperatures that is capable of sealing the steel from penetration; in addition, one highly refractory phase is necessary to hold the well powder in shape throughout the refining process before casting can take place. We herein propose a novel core–shell-structured composite particle that consists of a highly refractory core able to maintain the shape integrity when introduced into the nozzle taphole, while the low-melting shell material can react with molten steel to form viscous glass that fills into the particle interstices so that penetration of the liquid steel can be stopped. A SiC@$SiO_2$ core–shell structure has been prepared as a model material for the refractory filler sand, despite patent disclosure involving a coating operation of dissimilar materials in particulate form is available [6]. In this study, the formation of SiC@$SiO_2$ core–shell structure relies on an oxidation process that forms an adhesive interface at the SiC–$SiO_2$ interface. In comparison, a weak interface between dissimilar materials often results after binder burnout for the particulate coating method used in the patent [6].

## 2. Experimental details

### 2.1. Material and process

SiC particles (Kallex Corp., Taiwan) with a purity of 99.5% and an average particle size of 50 μm were used as the starting material. Steel ingot used was S1015S1 with major impurities including S (0.05 wt.%), P (0.02 wt.%), and Mn (0.01 wt.%). Oxidation of the SiC particles was carried out in a tube furnace (Lindberg Blue M, U.S.A.) at temperatures from 1100 to 1600 °C with 1 h isothermal holding in air atmosphere. The particles (about 10 g) were placed in an alumina crucible (40 mm × 20 mm × 15 mm) and were then inserted to the center of the tube furnace after reaching the pre-determined temperature. The heat-treatment temperature was monitored by an additional thermocouple placed just underneath the crucible, and the measured temperature difference over various locations of the crucible was found less than 2 °C. In addition, the oxidation temperatures mentioned above, e.g., 1100–1600 °C, were from the additional thermocouple reading placed close to the powders. The beginning of isothermal holding time was started when the ''real'' temperature reached the pre-determined oxidation temperature after the powdered sample was inserted into the furnace. Weight gain of the SiC particles was determined by an electrical balance with a precision of 0.1 mg after the oxidation in order to determine the amount of $SiO_2$ formed.

For the determination of reaction-layer thickness between steel and filler sand, the steel ingot was cut into pieces with a size of 5 mm × 5 mm × 3 mm (about 0.2 g apiece). The steel sample was then buried in loosely packed SiC@$SiO_2$ particles in the alumina crucible, and inserted quickly into the tube furnace maintained at 1500 °C for avoiding possible oxidation of the steel upon the temperature increase. The heat-treatment temperature was again monitored by the thermocouple placed just underneath the crucible. All the isothermal holdings were maintained at 10 min counting since the temperature returned back to 1500 °C after the sample insertion. The steel would react with the sands and the molten steel penetrated into the interstices of packing sands, leaving behind an empty mark after cooling. The reaction-layer thickness was defined (in the study) as the distance measured from the top of the packing sands to the bottom of the empty mark. Note that overall shrinkage of the packing sands was insignificant after the heat treatment. An industrial filler sand provided by the China Steel Corporation (Taiwan) was also tested for comparison purpose. The filler sand consists of chromite particles mixed with silica particles, in which the chromite/silica weight ratio is about 70/30 and the particle size mostly falls in a range from 300 to 600 μm.

### 2.2. Characterization

Morphology and elemental distribution of the SiC@$SiO_2$ particles were examined by field-emission scanning electron microscopy (FE-SEM, JSM 6700F, JOEL, Japan) equipped with an energy-dispersive X-ray spectroscopy (EDS, INCA Energy 400, Oxford, U.K.). Chemical composition at the particle-steel interface was determined semiquantitatively by EDS-ZAF analysis. Crystalline structure of the SiC@$SiO_2$ particles was characterized by X-ray diffractometry (XRD, MAC MXP-III, Japan) using CuKα radiation (λ = 1.5406 Å). In addition, the oxidized SiC particles were mixed with KBr powders and were then pressed into discs for X-ray photon electron spectroscopy (XPS, ULVAC-PHI, PHI 5000 VersaProbe/Scanning, U.S.A.) using 0.1 eV argon laser source. A scanning area of approximately 400 $\mu m^2$ was carried out on the particle assemblies for determining the Si 2p characteristic peak.

## 3. Results and discussion

### 3.1. Structural analysis

Fig. 1 shows morphology of the as-received SiC particles. The particles are mostly acicular and are of flake shape. The inset shows that only Si and C elements exist in the as-received form. In Fig. 2, XRD reveals that the as-received SiC particles are crystalline, and consists of rhombohedral α-SiC as the major phase and hexagonal 8H and polymorphs as the minor phase. Formation of quartz (JCPDF No. 46-1045) becomes apparent as the oxidation temperature was raised above 1200 °C. The diffraction intensity from the quartz appears to increase pronouncedly with the increasing oxidation temperature. This is especially true when the temperature was raised above 1500 °C.

Formation of the $SiO_2$ shell on the particle surface was verified by XPS analyses. As shown in Fig. 3(a), a high resolution scan of the Si 2p core-level region shows peaks at binding energies of 99.6 and 103.1 eV, respectively, for the

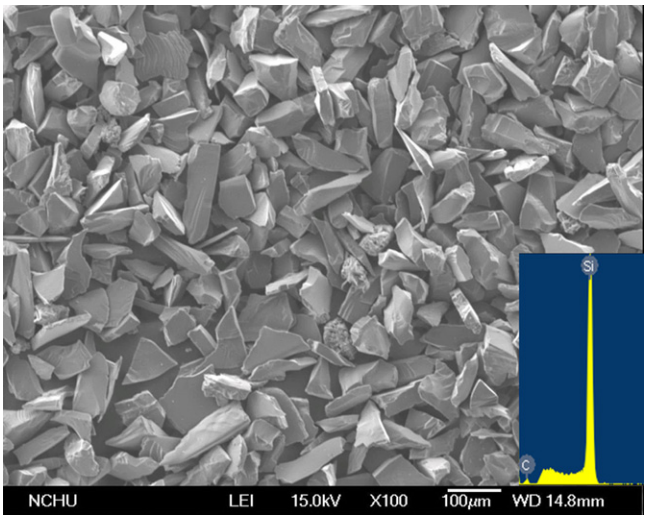


Fig. 1. Morphology of the as-received SiC particles. The inset shows Si and C elements from EDS analyses.

as-received SiC particles. The peak at 99.6 eV is attributable to the Si–Si bonding. However, deconvolution of the peak at 103.1 eV yields indeed three peak maxima, i.e., those at binding energies of 101.6, 103.1 and 103.6 eV corresponding to Si–C, Si–C–O and Si–O bonds, respectively [7–9]. This finding indicates that the as-received SiC particles contain some silicon oxycarbide (major) and natural silica (minor) near the surface. In comparison, the peak shifts markedly to 103.6 eV from 103.1 eV, while the peak ascribed to the Si-Si bonding remains unchanged for the SiC oxidized at 1600 °C (Fig. 3(b)). This reveals that the Si–O bond replaces the Si–C and Si–C–O bonds and becomes the predominant bonding configuration near the surface. This is in good agreement with the XRD finding.

### 3.2. $SiO_2$ weight gain and calculated shell thickness

Weight gain upon the $SiO_2$ formation and the estimated shell thickness are shown in Fig. 4(a). The weight increment is a

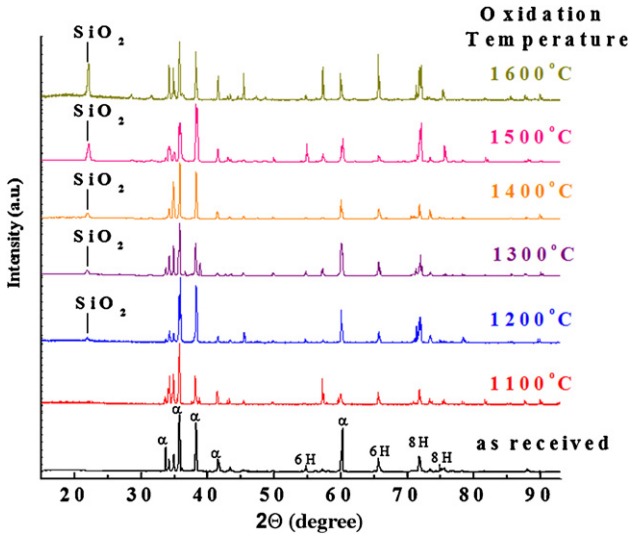


Fig. 2. XRD diffraction patterns of the as-received and oxidized SiC. The oxidation temperature varies from 1100 to 1600 °C.

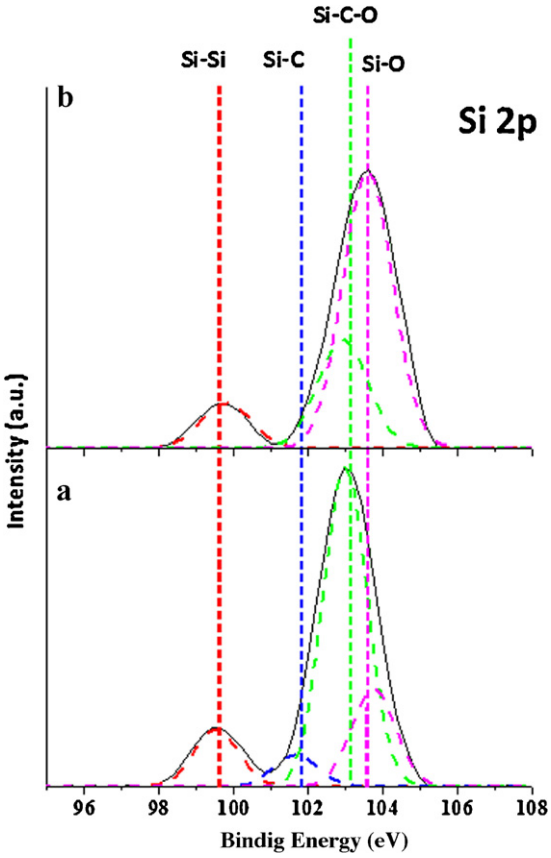


Fig. 3. Si 2p core-level spectra of (a) as-received and (b) 1600 °C oxidized SiC particles from XPS analyses.

merely 0.8 wt.% upon subjected to an oxidation temperature of 1100 °C. The weight gain then increases linearly with the temperature, and reaches 7.9 wt.% at 1600 °C. Thickness of the $SiO_2$ shell is estimated from the weight gain, assuming that the SiC particles were of spherical shape with a mean particle diameter of 50 μm. The morphology of the as-received SiC particles is indeed acicular flakes (Fig. 1); therefore, the estimate serves only as a first approximation. From Fig. 4(a), the shell thickness is found to increase linearly from 20 to 157 nm as the oxidation temperature increases from 1100 to 1600 °C. This finding includes at least two implications. First, the $SiO_2$ shell thickness can be tailored by tuning the oxidation temperature for the SiC@$SiO_2$ particles. Second, the calculated thickness is still relatively thin when compared to the particle diameter; therefore, a good portion of the particle remains intact (i.e., SiC remains as the major chemical composition) and is hence capable of providing a mechanical strength sufficient for maintaining the shape integrity as a whole when used as a filler sand at elevated temperatures.

The activation energy ($E_a$) of the SiC oxidation is estimated from the Arrhenius equation:

$$k = k_o \exp^{(-E_a/RT)} \quad (1)$$

where $k$ is the rate constant, $R$ is the gas constant, $k_o$ is a constant that can be determined experimentally, and $T$ is the oxidation temperature in Kelvin. In Fig. 4(b), a linear

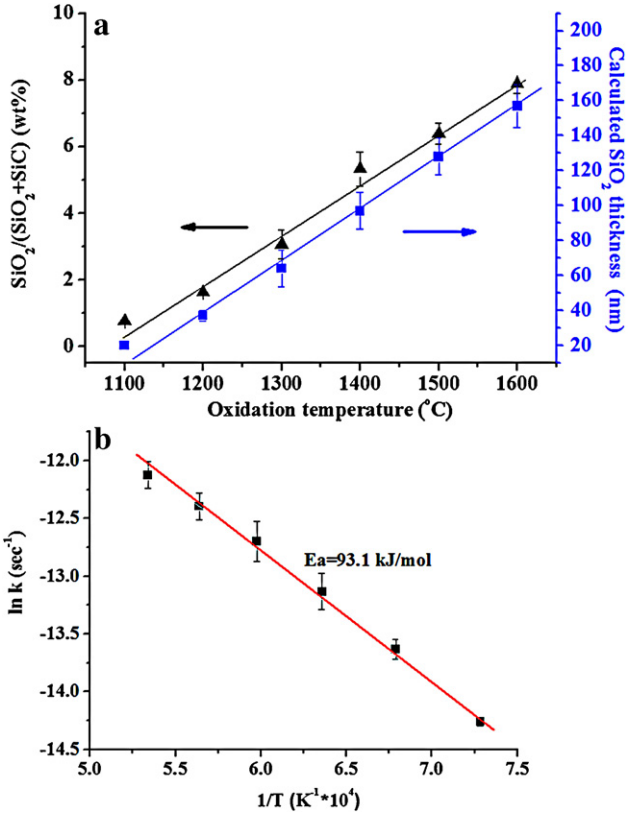


Fig. 4. (a) The $SiO_2$ weight gain over the oxidation temperatures examined. (b) The Arrhenius plot for determining the activation energy for the SiC oxidation.

relationship is found, suggesting that the oxidation is a first order reaction. The calculated $E_a$ is 93.1 kJ/mol. In comparison, Das et al. [10] have reported an activation energy of 179 kJ/mol for SiC oxidation, which is substantially higher than that found in this study. The difference may stem from the surface chemistry, impurity concentration and composition of the SiC particles examined. In addition, Ramberg et al. [11] have found that Si-terminated and C-terminated faces exist on the surface of SiC single crystals. The activation energy required for oxidation to occur on the Si-terminated faces was $E_a = 292$ kJ/mol; while, $E_a = 99$ kJ/mol for the C-terminated faces. The reduced activation energy found in this study might also stem from the abundance of C-terminated faces in the polycrystalline SiC particles examined.

### 3.3. A laboratory test on the molten steel penetration

Fig. 5 shows a line scan of elemental distributions at six positions, each spaced 5 μm apart, across the interface between SiC@$SiO_2$ and steel after 1500 °C soaking. From the EDS-ZAF analysis, iron (Fe) atoms appear to have diffused into the SiC@$SiO_2$ particle since an increasing Fe concentration is found from the SiC@$SiO_2$ region toward the steel, along with a conjugating decrease of Si concentration on the opposite direction. No apparent cracking is seen found from the SiC@$SiO_2$, suggesting that an adhesive interface exists after the oxidation operation in preparing the core–shell structure.

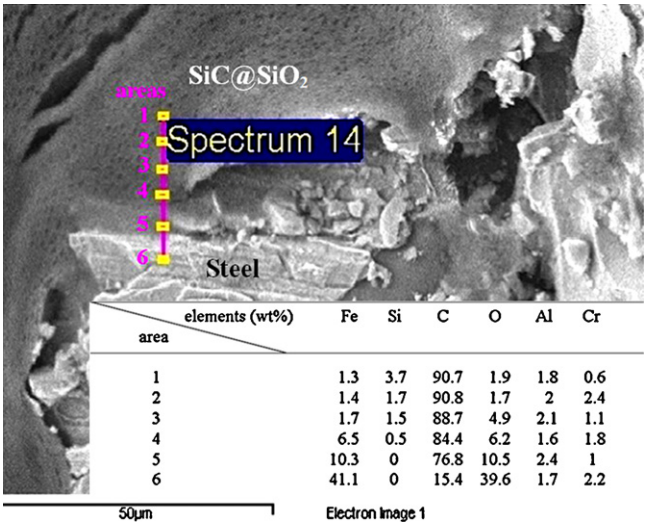


| area | elements (wt%) | Fe | Si | C | O | Al | Cr |
|---|---|---|---|---|---|---|---|
| 1 | | 1.3 | 3.7 | 90.7 | 1.9 | 1.8 | 0.6 |
| 2 | | 1.4 | 1.7 | 90.8 | 1.7 | 2 | 2.4 |
| 3 | | 1.7 | 1.5 | 88.7 | 4.9 | 2.1 | 1.1 |
| 4 | | 6.5 | 0.5 | 84.4 | 6.2 | 1.6 | 1.8 |
| 5 | | 10.3 | 0 | 76.8 | 10.5 | 2.4 | 1 |
| 6 | | 41.1 | 0 | 15.4 | 39.6 | 1.7 | 2.2 |

Fig. 5. An EDS line scan across the interface of SiC@$SiO_2$ and steel. The inset shows elemental distribution in weight ratio at 6 positions on the line scan.

Oxidation of the steel yet still occurs over the soaking time used, despite the use of quick insertion operation for the steel-loaded samples.

Thickness of the reaction layer varies from 1.8 to 5.4 mm in Fig. 6 when the SiC@$SiO_2$ particles were used in the molten-steel infiltration bench-test. The reaction-layer thickness scales with the $SiO_2$ content, indicating that the penetration depth can be tailored by adjusting the $SiO_2$ shell thickness. In Fig. 6, the thickness can be tuned to a level identical to or less than that of the commercial chromite-based filler sand tested under identical conditions. In practice, the filler sands used in taphole nozzle of typical ladle-steel refining process usually involve a working temperature above 1600 °C with a duration time ranging from 30 to 60 min. At such circumstances, further growth of the $SiO_2$ layer on the SiC@$SiO_2$ particles are

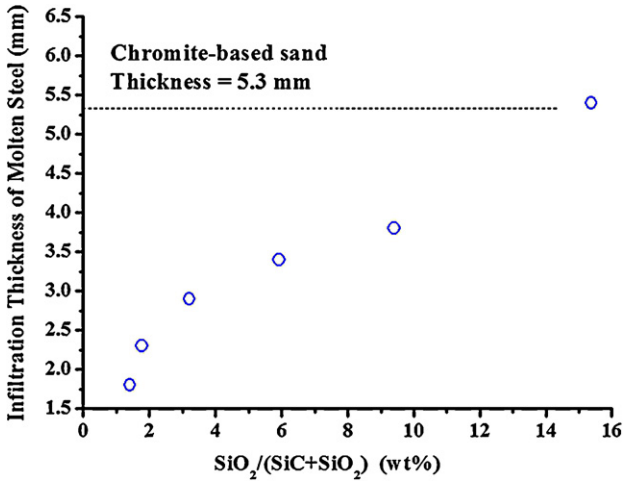


Fig. 6. Reaction-layer thickness for the molten steel to infiltrate into the interstices of loosely packing SiC@$SiO_2$ particles at 1500 °C. The SiC@$SiO_2$ particles were oxidized at 1100–1600 °C in ambient air before the reaction bench-test takes place.

inevitable since that air existing in the particle interstices as well as the dissolved oxygen in the penetrating molten steel both provide oxygen for the $SiO_2$ formation. Taking these into consideration, SiC@$SiO_2$ composite particles with an adjustable $SiO_2$ shell thickness, so that a tailored infiltration depth of molten steel, become indeed more attractive in high-temperature refractory use than the conventional mixture-type filler sand, since the $SiO_2$ layer thickness can be adjusted to a large extent (see Fig. 6) by tuning the heat-treatment process (i.e., temperature and time) so that the composite structure can be tailored to fit the practical operation need. An additional merit of using the SiC@$SiO_2$ particles includes that particle segregation arising from mixing of dissimilar particles of different compositions, sizes, and densities can be avoided when the core–shell-structured composite particles are used.

## 4. Conclusion

Core–shell-structured SiC@$SiO_2$ particles with an adhesive interface between the dissimilar phases were prepared by a facile oxidation process from SiC particles at elevated temperatures. Formation of the $SiO_2$ shell on the surface of SiC particles was confirmed by XRD and XPS analyses; in addition, the thickness of the $SiO_2$ shell could be tailored by varying the oxidation temperature. For the SiC particles examined, the silica weight-ratio increased from 0.8 to 7.9 wt.% when the oxidation temperature was increased from 1100 to 1600 °C. This silica formation was equivalent to a calculated shell thickness of 20–157 nm. In our laboratory bench-test, the infiltration thickness for molten steel to react with the composite sand could be tuned by the $SiO_2$ shell thickness, revealing possible use of the composite sand for replacing conventional mixture-typed refractory sand in high-temperature metallurgical applications.

## Acknowledgments

We are indebted to Dr. B.W. Lin for providing the SiC powder. Financial support from the Ministry of Economic Affairs (Taiwan) under contract no. 98-EC-17-A-08-S1-117 is gratefully acknowledged.

## References

[1] H.-C. Pan, Y.-C. Ko, Constituents and characterization of packing sand for sliding gate systems for steel ladles, Am. Ceram. Soc. Bull. 60 (1981) 736–739.
[2] Y.T. Chien, H.C. Pan, Y.C. Ko, Preparation and performance of packing sands for sliding-gate systems for steel ladles, Ironmak. Steelmak. 9 (1982) 252–257.
[3] H. Bai, B.G. Thomas, Effect of clogging, argon injection, and continuous casting conditions on flow and air aspiration in submerged entry nozzles, Metall. Mater. Trans. B 32 (2001) 707–722.
[4] T. Kono, Y. Fukuhisa, Improvement of opening ratio without burning by oxygen on ladle sliding nozzles, Taikabutsu 30 (1978) 638–642.
[5] T.-F. Lee, Y.-C. Ko, Softening and melting behavior of feldspar for application in packing sands for sliding gate systems for steel ladles, Am. Ceram. Soc. Bull. 61 (1982) 737–740.
[6] T. Nishio, T. Katayose, Filler material for filling an outlet aperture of a casting ladle or similar container and a process for producing the filler material, U.S. Patent 4,667,858.
[7] O. Renault, R. Marlier, N.T. Barrett, E. Martinez, T. Baron, M. Gely, B. De Salvo, Modeling the XPS Si 2p core-level intensities of silicon nanocrystals for determination of oxide shell thickness, Surf. Interface Anal. 38 (2006) 486–488.
[8] G.M. Renlund, S. Prochazka, R.H. Doremus, Silicon oxycarbide glasses: Part II. Structure and properties, J. Mater. Res. 6 (1991) 2723–2734.
[9] A. Avila, I. Montero, L. Galán, J.M. Ripalda, R. Levy, Behavior of oxygen doped SiC thin films: an X-ray photoelectron spectroscopy study, J. Appl. Phys. 89 (2001) 212–216.
[10] D. Das, J. Farjas, P. Roura, Passive-oxidation kinetics of SiC microparticles, J. Am. Ceram. Soc. 87 (2004) 1301–1305.
[11] C.E. Ramberg, G. Cruciani, K.E. Spear, R.E. Tressler, Passive-oxidation kinetics of high-purity silicon carbide from 800 °C to 1100 °C, J. Am. Ceram. Soc. 79 (1996) 2897–2911.